

## Supplementary Information

### **A reversible self-assembled molecular layer for lithium metal batteries with high energy/power densities at ultra-low temperatures**

Weili Zhang<sup>1,3,4</sup>, Yang Lu<sup>1,4</sup>, Qingbin Cao<sup>1,4</sup>, Hao Liu<sup>1</sup>, Qingqing Feng<sup>3</sup>, Pan Zhou<sup>1</sup>,  
Yingchun Xia<sup>1</sup>, Wenhui Hou<sup>1</sup>, Shuaishuai Yan<sup>1</sup>, Kai Liu<sup>\*1,2,3</sup>

<sup>1</sup>Department of Chemical Engineering, Tsinghua University, China

<sup>2</sup>Ordos Laboratory, Inner Mongolia, 017000, China

<sup>3</sup> Tsinghua University Hefei Institute for Public Safety Research, China

<sup>4</sup>These authors contributed equally: Weili Zhang, Yang Lu, Qingbin Cao

\*Corresponding author. E-mail: [liukai2019@tsinghua.edu.cn](mailto:liukai2019@tsinghua.edu.cn)

This file includes:

Experimental and Computational Methods

Figs. S1 to S45

Tables S1

References 1-2

## Methods

**Materials.** Battery-grade Lithium Bis(fluorosulfonyl)imide (LiFSI) (>99.9%), Tris(trimethylsilyl)phosphate (TMSP) and 1 M LiPF<sub>6</sub>/EC+DEC (1:1 by volume) was purchased from DodoChem. Tetrahydrofuran (THF) (>99.9%), Sodium perfluorooctanoate (NaPFO) and Perfluorooctane (PF) were purchased from Shanghai Aladdin Bio-Chem Technology Co., LTD. Trimethyl-1-propanaminium iodide (TTPI) were purchased from Shanghai Macklin Biochemical Technology Co., Ltd. The synthesis route for Trimethyl-1-propanaminium Bis(fluorosulfonyl)imide (TTPFSI) is as follows: Trimethyl-1-propanaminium iodide (TTPI) and LiFSI are reacted in a molar ratio of 1:1.05 in an aqueous solution through ion exchange reaction. The crude product TTPFSI precipitates in the aqueous solution. The crude product is then purified by extraction using dichloromethane and water. The final product is transferred to a glove box after being placed in a vacuum oven at 80°C for 24 hours. By dissolving a predetermined amount of lithium salt (LiFSI) into a solvent of interest (THF) and stirring, forming the 1.0 M LiFSI/THF, and then 0.5 wt% of NaPFO was added to obtain the final electrolyte 1.0 M LiFSI-NaPFO/THF. Metallic Li foil was purchased by China Energy Lithium Co., LTD. N-Methyl-2-pyrrolidone (NMP), LiNi<sub>0.8</sub>Mn<sub>0.1</sub>Co<sub>0.1</sub>O<sub>2</sub> (NMC811), LiFePO<sub>4</sub> (LFP) were purchased from Nanjing Mojiesi Energy Technology. Cathode NMC811/LFP laminates were prepared by laying a mixture of 90 wt% NMC811 or LFP particles, 5 wt% super-p and 5 wt% PVDF (5.0 wt% NMP) on a carbon coated aluminum foil current collector and dried at 100 °C under vacuum before cell fabrication. The Full cell assembly: NMC811

cathode has a capacity of about 2.6 mAh g<sup>-1</sup>, a 40 μm thick lithium metal is cut into small discs with a diameter of 14 mm to serve as the negative electrode, with an N/P ratio of approximately 4.3. Industry-level 500 mAh/3300 mAh Li||NMC811 pouch cells (cathode loading: 20.69 mg cm<sup>-2</sup>, 4.0 mAh cm<sup>-2</sup>, Anode: 50 μm Li foil, N/P=1.26) were purchased from LI-FUN Technology.

**Characterizations.** The surface morphology of lithium deposition was characterized by a JSM-7401F scanning electron microscopy (SEM). The JEM-2100 Plus transmission electron microscope (TEM) at an accelerating voltage of 200 kV was conducted to characterize CEI layers coating on cathode NMC811 particles. The SEI/CEI chemical composition information were measured by using X-ray photoelectron spectroscopy (XPS, ESCALAB Xi+) sputtering at different depths. The C1s peak at 284.6 eV was used as the reference for all binding-energy values. The ionic conductivities of the electrolytes at different temperatures were measured by electrochemical impedance spectroscopy (EIS) measurements with two polished 316 platinum plate electrodes symmetrically placed at a set distance in the electrolyte solutions.

**Electrochemical coupled-attenuated total reflection surface-enhanced infrared absorption spectroscopy (EC-ATR-SEIRAS).** EC-ATR-SEIRAS measurements were conducted by Bruker Vertex 70 FTIR spectrometer. The electrochemical cell included three electrodes, the NMC811-coated substrate as working electrode, the platinum wire as the counter electrode, and the Li metal as the reference electrode. The working electrode is firstly deposited a 100nm Au film onto the reflective surface

of the Si prism through vacuum evaporation, and then coated with a layer of ultra-thin NMC811 slurry with CMC and SBR as binders. In order to ensure pure capacitive behavior throughout the test process and exclude any irreversible Faraday reaction including the formation of CEI, we set the voltage range to 3.0-3.6 V vs. Li/Li<sup>+</sup>. The charge-discharge process employs the sweep-step function method. Upon reaching a certain set voltage during charging or discharging, the system maintains this voltage for 2 minutes. This is done to achieve chemical and electrical equilibrium in the battery system and to allow sufficient time for infrared testing.

**In-situ electrochemical coupled-quartz crystal microbalance (EC-QCM).**

EC-QCM measurements were conducted by using a QSense Explorer (Biolin Scientific AB, Sweden) with copper-coated quartz crystal sensor chips (QSX 313, Biolin Scientific AB, Sweden). The electrochemical cell dedicated to the EC-QCM uses a three-electrode configuration in which the Pt plate serves as the counter electrode, the Li metal serves as the reference electrode, and nickel-coated gold chip serves as the working electrode. Any changes occurring on the working electrode surface in the electrochemical environment (GCD test, voltage range 3.0-3.6 V vs. Li/Li<sup>+</sup>) can be measured in real time by monitoring the dissipation (D) changes of the chip. Please see Supplementary Note 2 for details.

**In situ electrochemical-atomic force microscopy (EC-AFM).** Combining AFM (Bruker, Multimode 8 with Nanoscope V controllers) with electrochemical workstation (CHI660E) for in situ AFM electrochemical experiments. The self-made in-situ electrochemical cell adopts a three-electrode system, in which the working

electrode is a silicon wafer coated with 100nm gold film on the surface, and both the opposite electrode and the reference electrode are platinum. A silicon AFM probe (Bruker,  $k = 26 \text{ N m}^{-1}$ ,  $f_0 = 300 \text{ kHz}$ ) was immersed into the sealed three-electrode electrochemical cell to monitor the morphology evolution and mechanical property feedback of the interface layer on the working electrode during the electrochemical test (3.0 V-3.6 V vs. Li/Li<sup>+</sup>) in the mode of PeakForce Quantitative Nano-Mechanics. To ensure pure capacitive behavior throughout the test process and exclude any irreversible Faraday reaction including the formation of CEI, we set the voltage range to 3.0 V-3.6 V vs. Li/Li<sup>+</sup>. Please see Supplementary Note 3 for details.

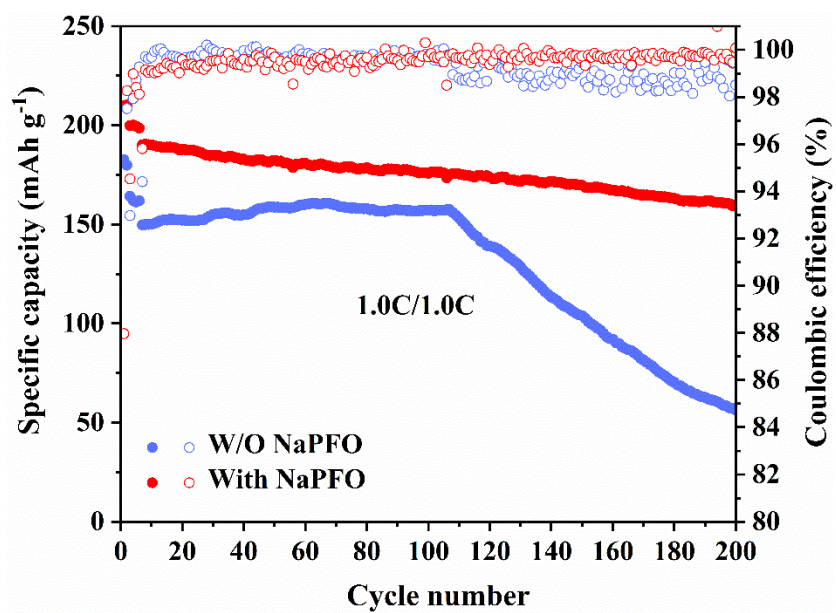
**Electrochemical measurements.** The electrochemical performances of the Li||Cu, Li||Li, Li||NMC batteries were examined using 2,032-type coin cells conducted on a battery test station (LANHE CT3001A). For low temperature discharge experiments at different temperatures, the battery was charged at a current density of 0.5 C under room temperature and discharged at a current density 0.1 C under different temperatures. All cells rested at different temperatures for 2 hours to achieve temperature equilibrium and then subjected to electrochemical test. The Li||NMC811 full cells utilized of 2.6 mAh cm<sup>-2</sup> NMC811 cathodes with 40 μm Li counter electrodes, N/P = 4. The power density P (W kg<sup>-1</sup>) is obtained by dividing the energy density W (Wh kg<sup>-1</sup>) by the discharge time t (s).

**Computational Methods.** Two simulation boxes consisting of 100 LiFSI with and without 10 NaPFO dispersed in 1233 THF solvent molecules were constructed. The atomistic force field we used was the AMBER force field<sup>1</sup>. The Lorentz-Berthelot

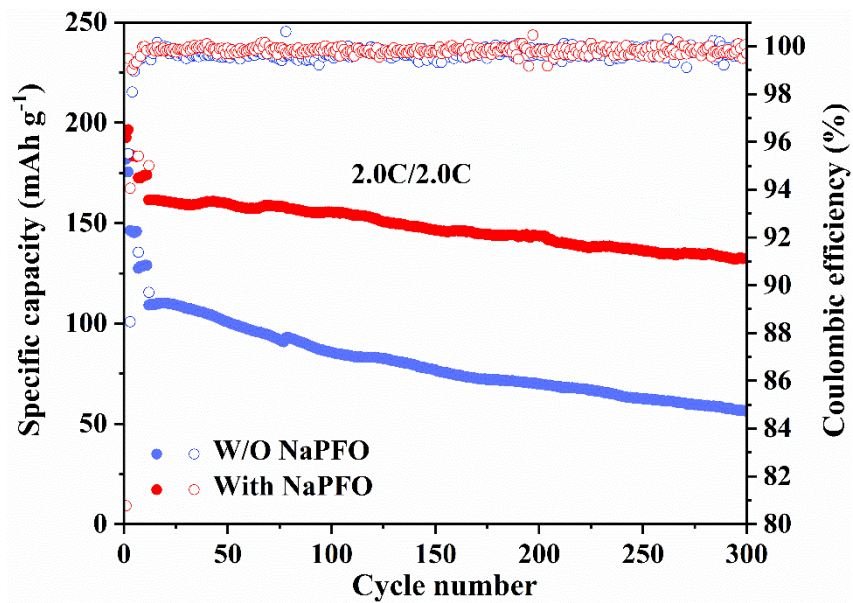
combination rule was utilized to acquire the cross-interaction parameters between different atom types.

Classical molecular dynamics (MD) simulations were carried out using GROMACS package with periodic boundary conditions (54). Verlet leapfrog integration algorithm with a time step of 1.0 fs was applied to integrated the equations for the motion of all atoms. A cutoff of 1.6 nm was adopted for L-J interactions, and the long-range electrostatic interactions were treated by the particle-mesh Ewald (PME) summation method. All simulation systems were first energetically minimized by steepest descent algorithm, then annealed gradually from 600 K to room temperature (300 K) within 12 ns. Afterward, to control the temperature at 300 K and the pressure at 1 atm, we equilibrated aforementioned systems in an isothermal-isobaric (NPT) ensemble for 15 ns using a Nosé-Hoover thermostat and a Parrinello-Rahman barostat with time coupling constants of 0.4 and 0.2 ps, respectively. Finally, canonical ensemble (NVT) simulations were performed for 40 ns, while system coordinates were saved every 100 fs for deeper structural and dynamical analysis.

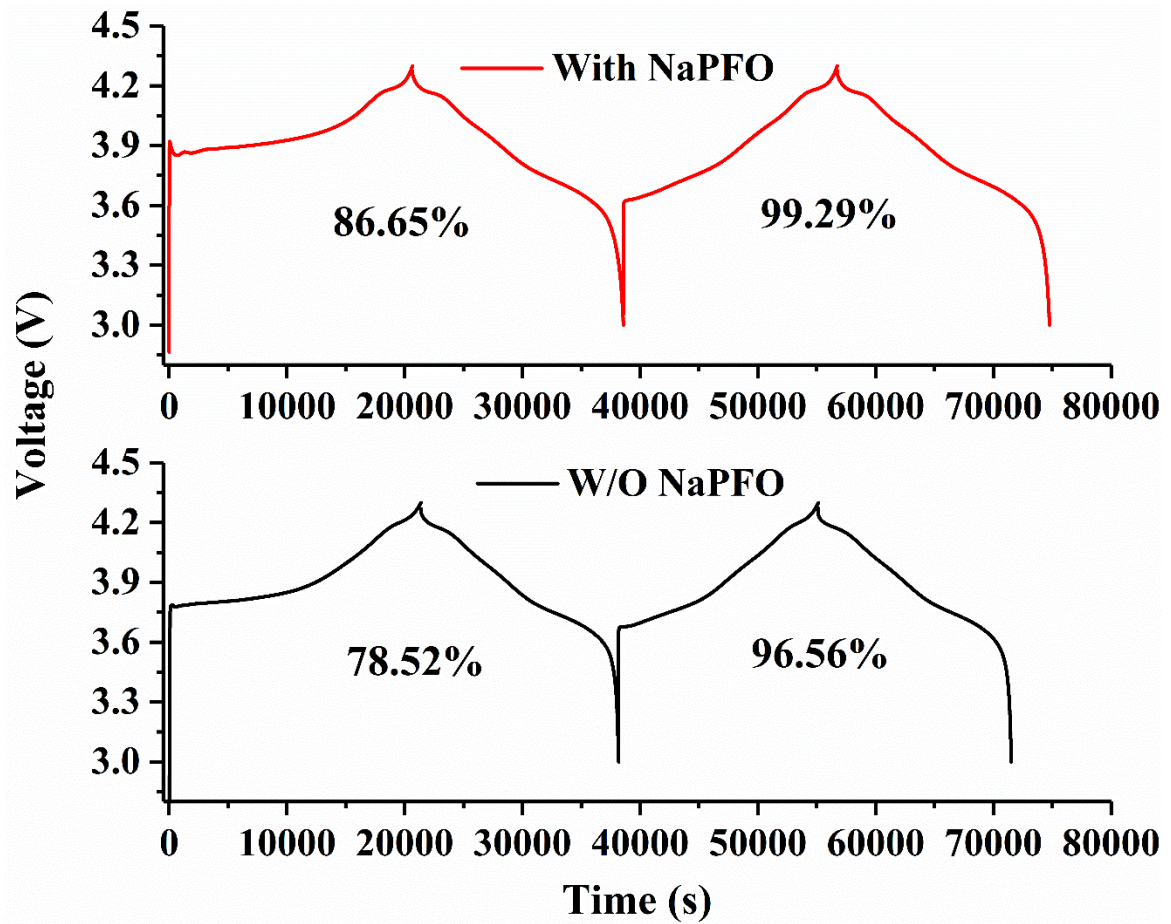
Representative solvation structures obtained from MD simulation trajectories were used as initial configurations for quantum chemistry calculations with the Gaussian 16 package<sup>2</sup>. DFT calculations were conducted at the B3LYP/6-311+G(d) level to optimize geometry, and binding energies were calculated with the Møller-Plesset second-order perturbation method and the correlation-consistent polarized valence cc-pVTZ(-f) basis set.



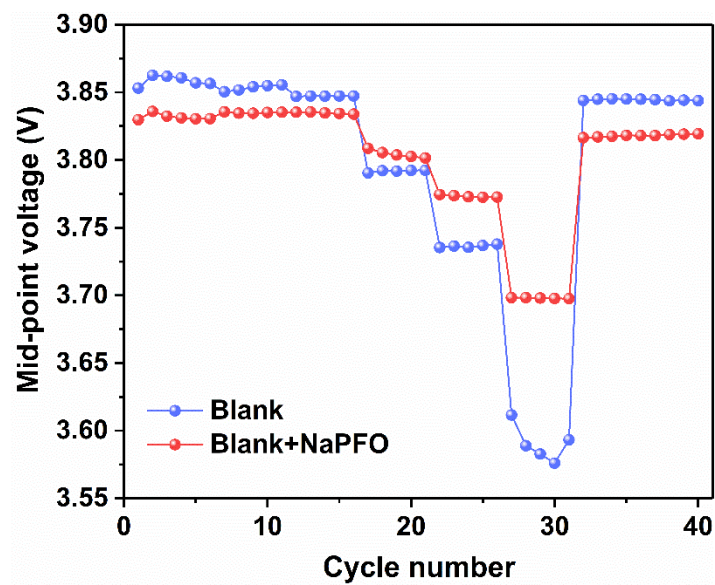
**Fig. S1.** Long-term cycling performance of Li||NMC811 cells using LiFSI/THF and LiFSI-NaPFO/THF at 1.0 C rate.



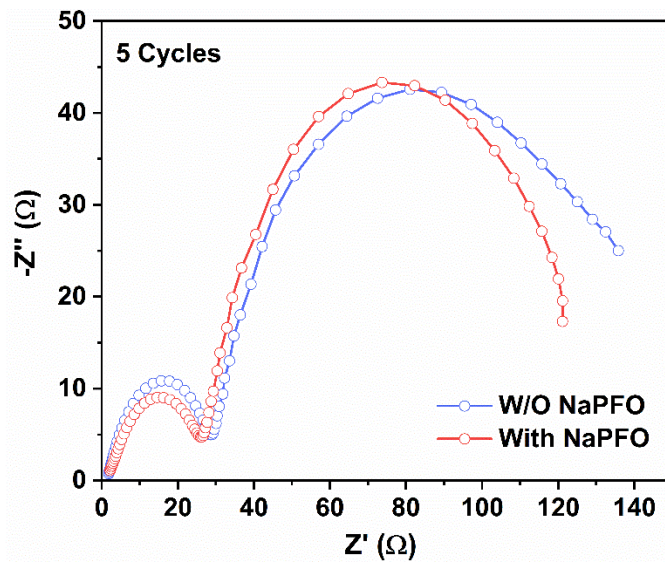
**Fig. S2.** Long-term cycling performance of Li||NMC811 cells using LiFSI/THF and LiFSI-NaPFO/THF at 2.0 C rate.



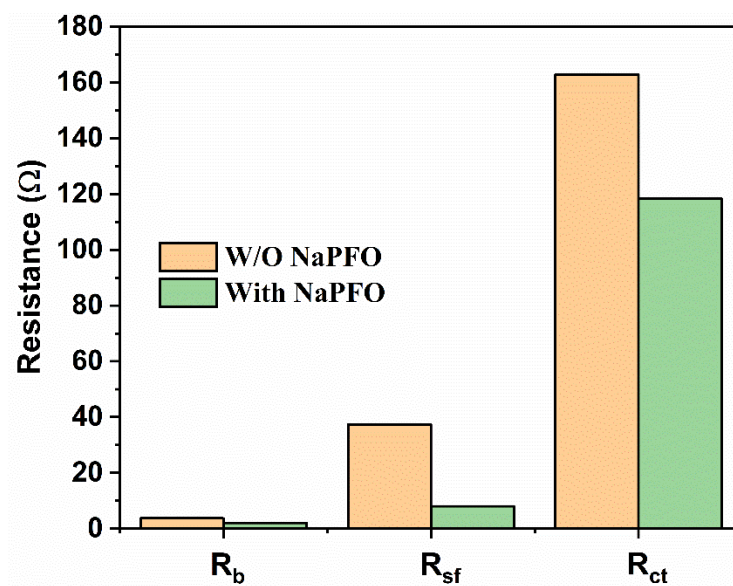
**Fig. S3.** Formation cycle of Li||NMC811 cells using LiFSI/THF and LiFSI-NaPFO/THF at 0.2 C rate.



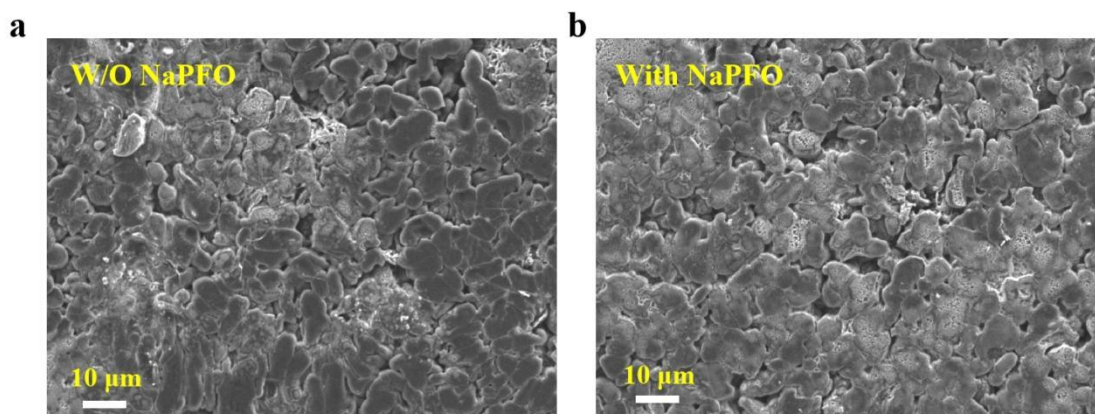
**Fig. S4.** The mid-point voltage of the Li||NMC811 cell cycled in both electrolytes from 0.2 C to 10.0 C rate.



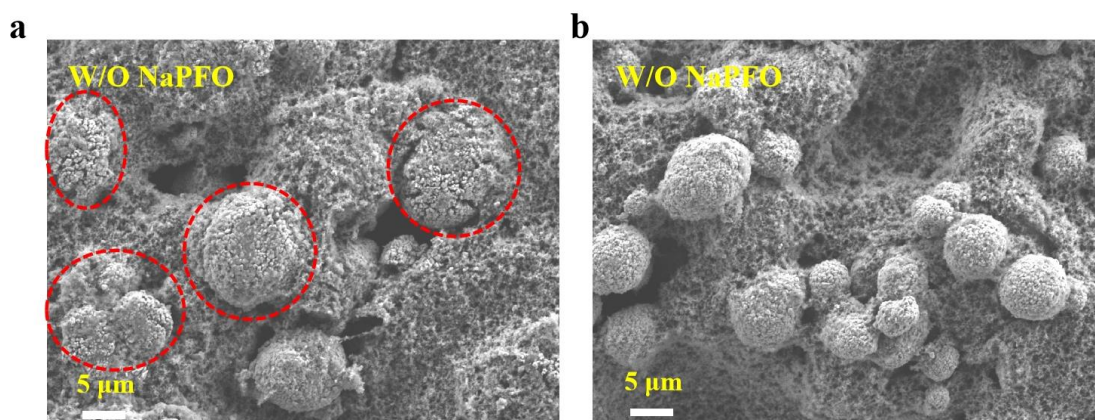
**Fig. S5.** Electrochemical impedance spectroscopy (EIS) tests of the Li||NMC811 cells using different electrolytes after 5 cycles.



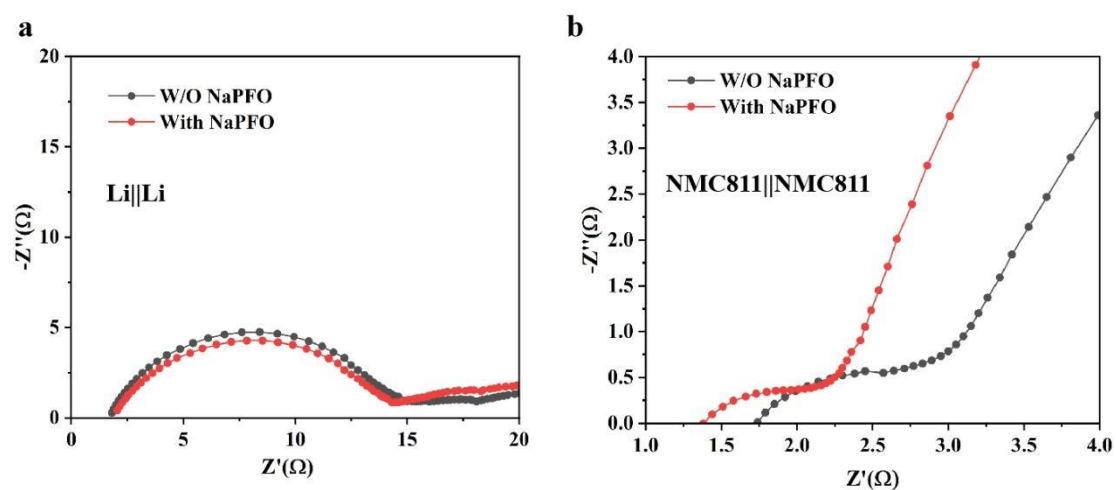
**Fig. S6.** Quantitative analysis of EIS after 100 cycles by fitting the equivalent circuit model.



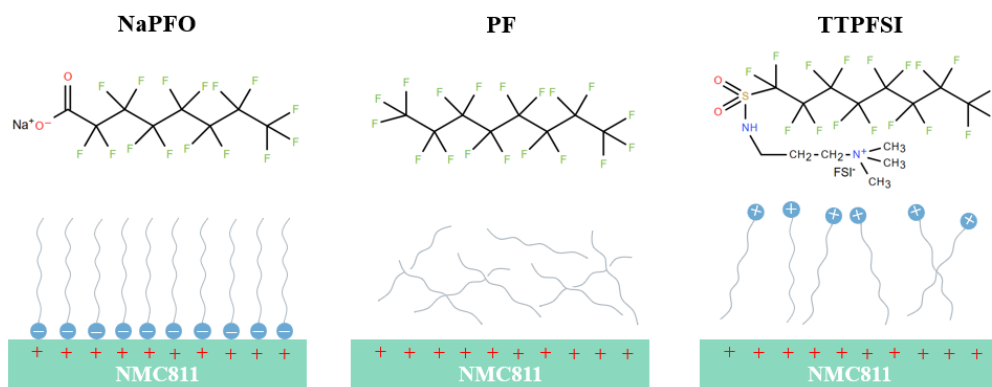
**Fig. S7.** SEM images of the lithium metal morphology from the cell after 100 cycles.



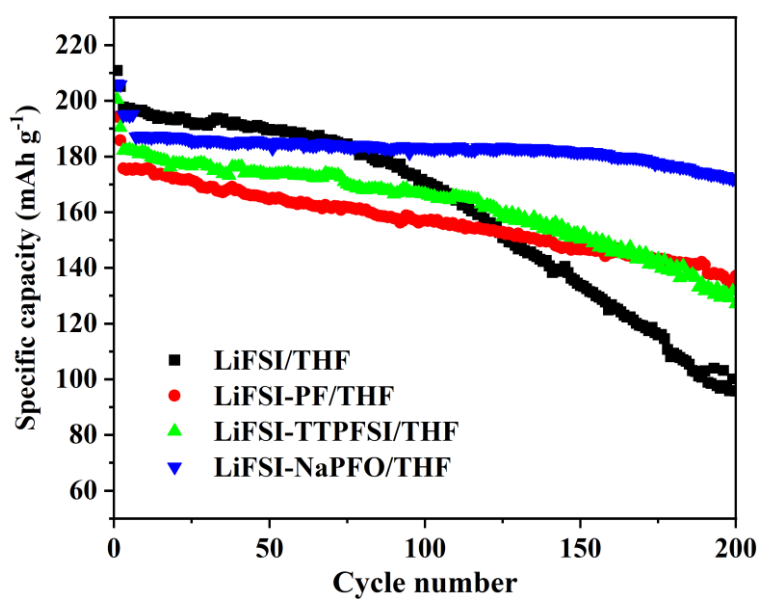
**Fig. S8.** SEM images of the NCM811 cathode morphology from the cell after 100 cycles.



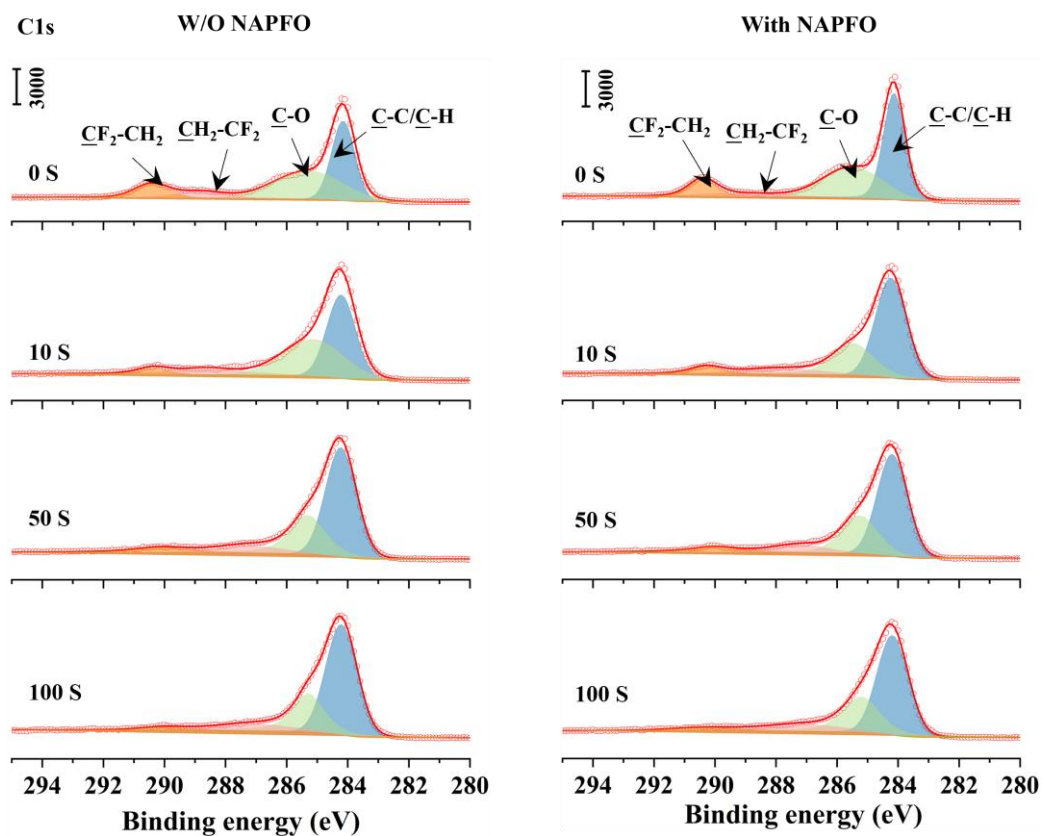
**Fig. S9.** Impedance spectra of reassembled Li||Li and NMC811||NMC811 symmetric cells.



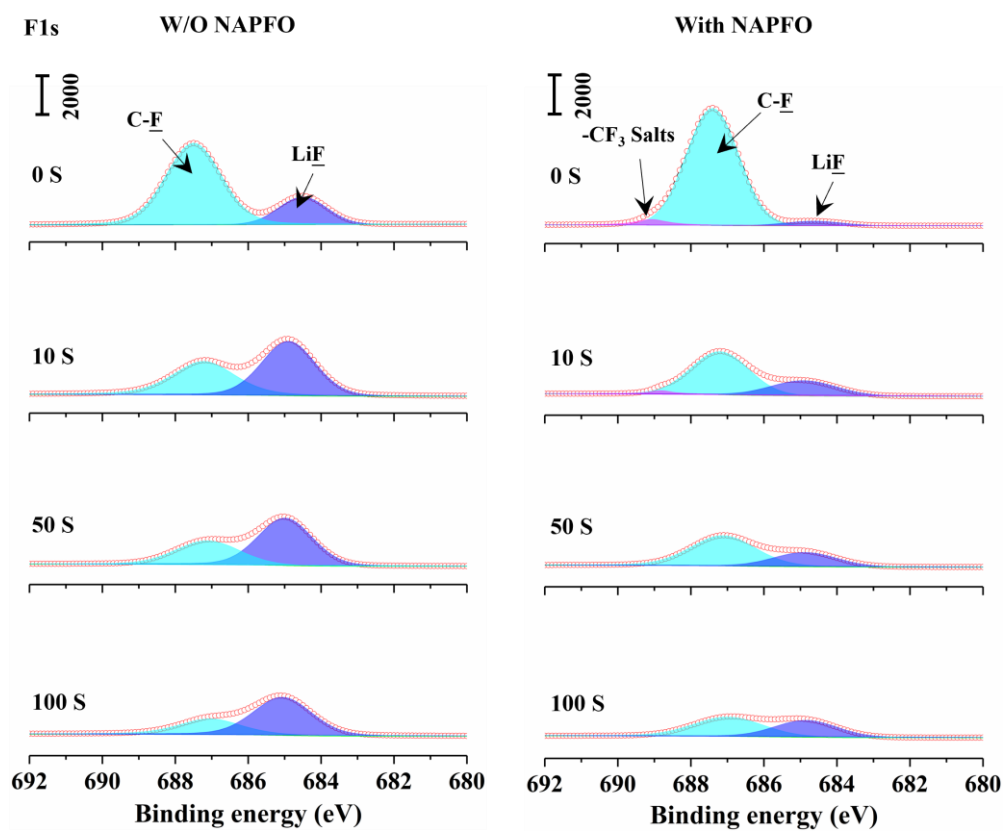
**Fig. S10.** Schematic diagram of molecular structures of three different surfactants and their working mechanisms on the surface of the polarized cathodes.



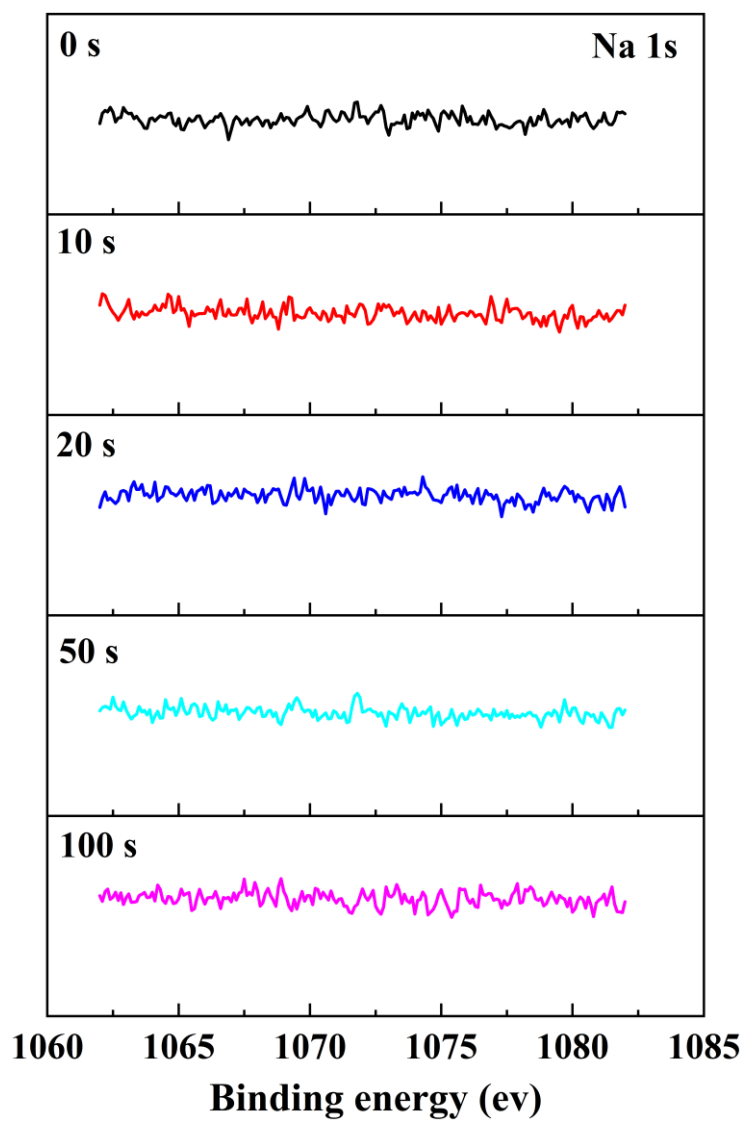
**Fig. S11.** Long-term cycling performance of Li||NMC811 cells using LiFSI/THF, LiFSI-PF/THF, LiFSI-TTPFSI /THF, LiFSI-NaPFO/THF at 1.0 C rate.



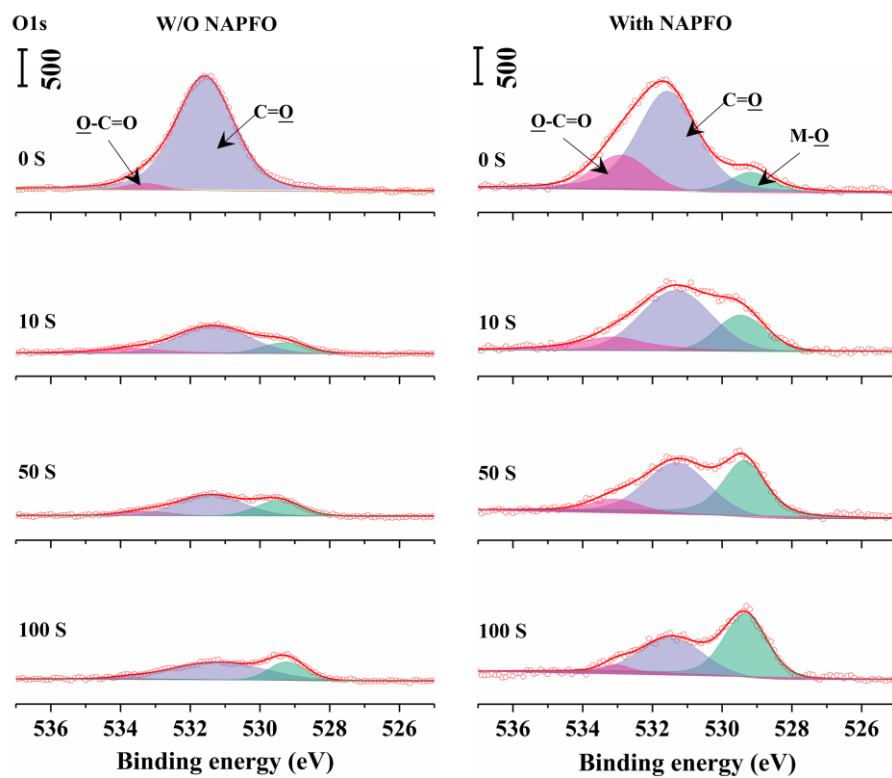
**Fig. S12.** XPS depth profiles of C 1s of CEI formed on NMC811 surface after 20 cycles at 0.5 C in Li||NMC811 coin cells with LiFSI/THF and LiFSI-NaPFO/THF.



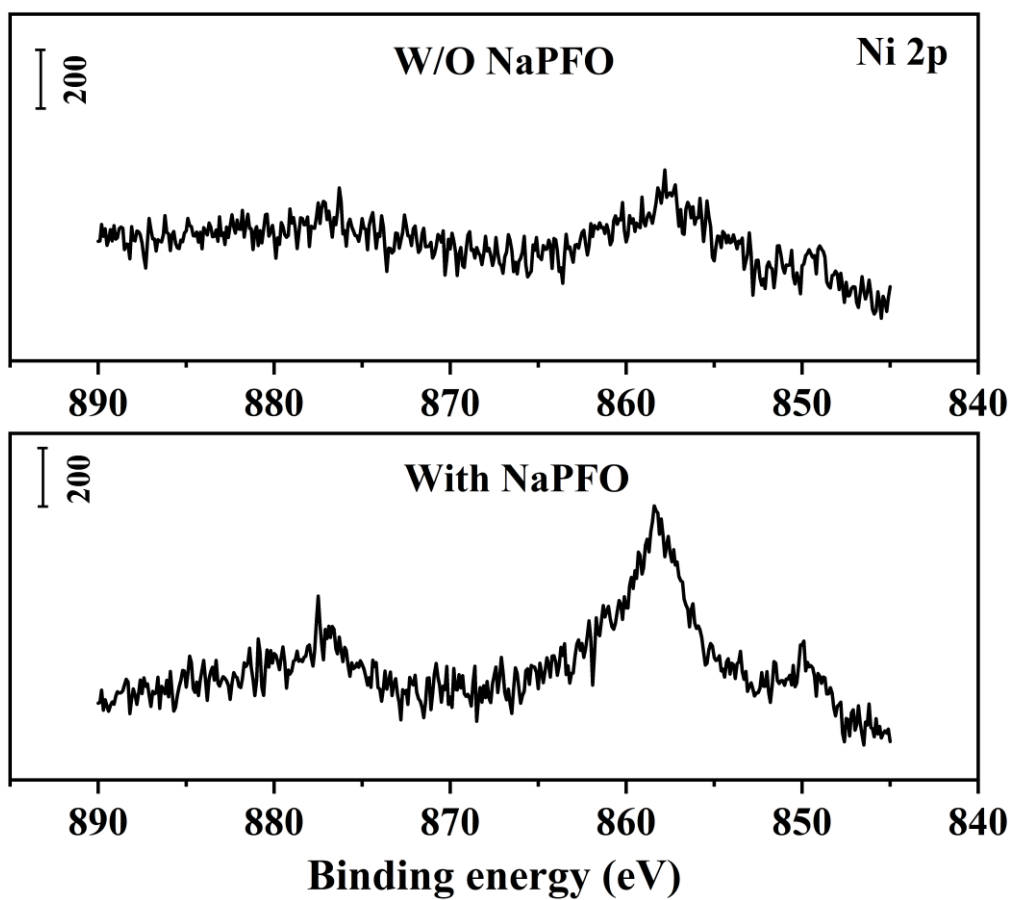
**Fig. S13.** XPS depth profiles of F1s of CEI formed on NMC811 surface after 20 cycles at 0.5 C in Li||NMC811 coin cells with LiFSI/THF and LiFSI-NaPFO/THF.



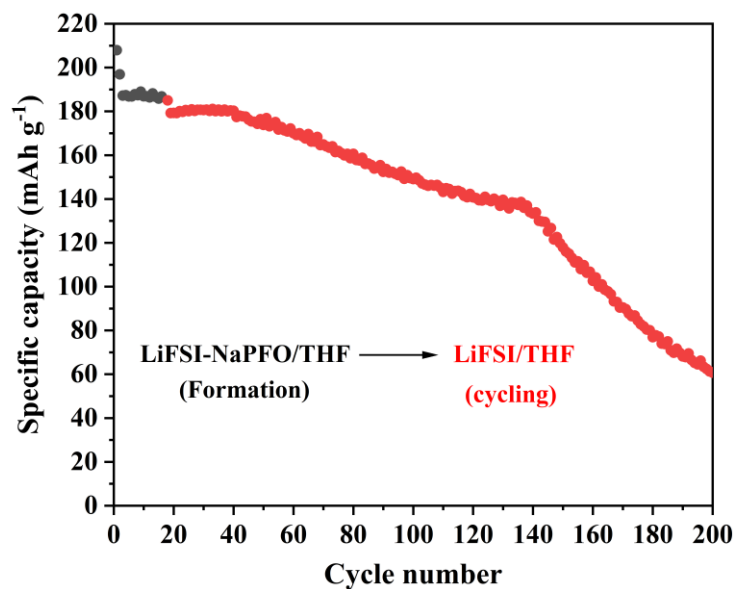
**Fig. S14.** XPS depth profiles of Na 1s of CEI formed on NMC811 surface after 20 cycles at 0.5 C in Li||NMC811 coin cells with LiFSI-NaPFO/THF.



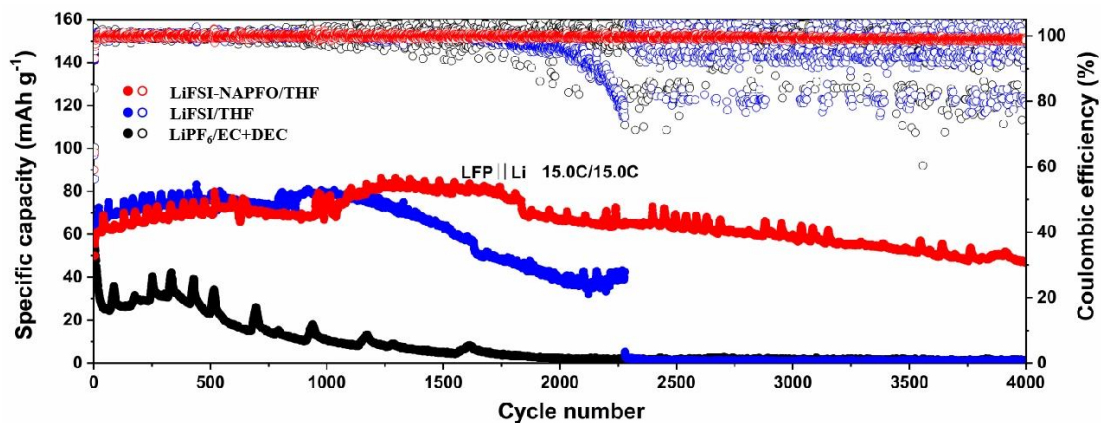
**Fig. S15.** XPS depth profiles of O1s of CEI formed on NMC811 surface after 20 cycles at 0.5 C in Li||NMC811 coin cells with LiFSI/THF and LiFSI-NaPFO/THF.



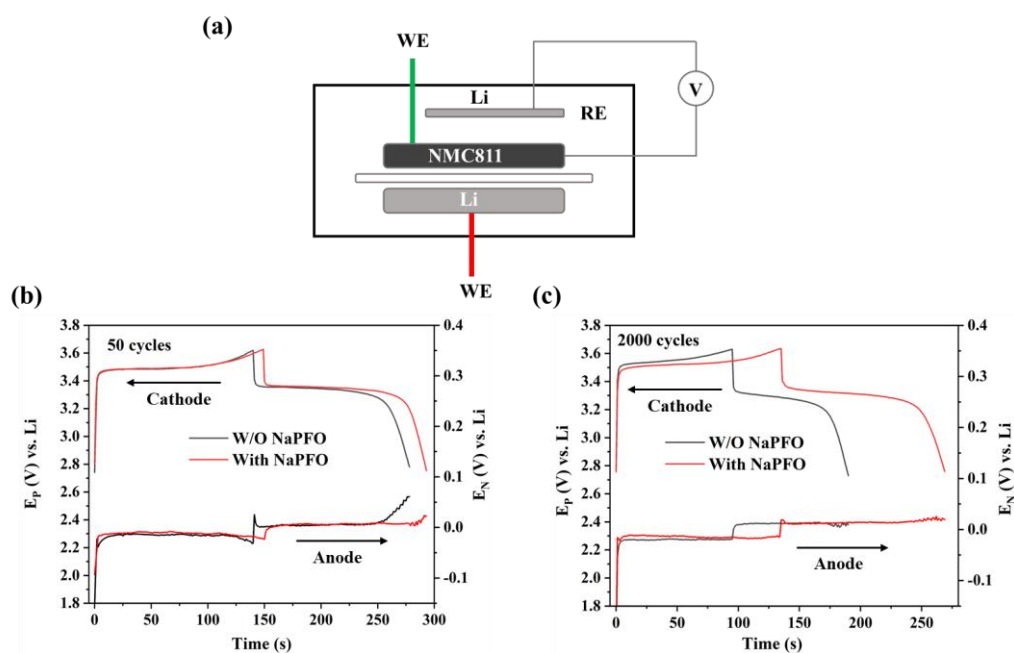
**Fig. S16.** XPS depth profiles of Ni 2p of CEI formed on NMC811 surface after 20 cycles at 0.5 C in Li||NMC811 coin cells with LiFSI/THF and LiFSI-NaPFO/THF.



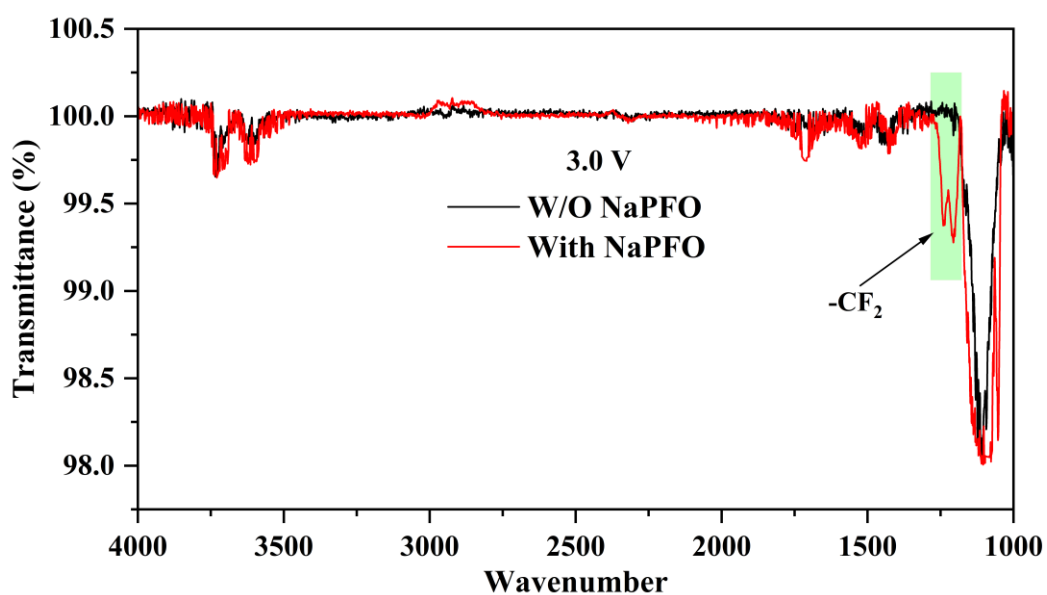
**Fig. S17.** Voltage profiles of the Li||NMC811 cell using 1.0 M LiFSI/THF after cycled 15 cycles in LiFSI-NaPFO/THF. The disassembled NMC811 cathode, Li anode and separator were washed with THF solvent for several times to remove residual lithium salt.



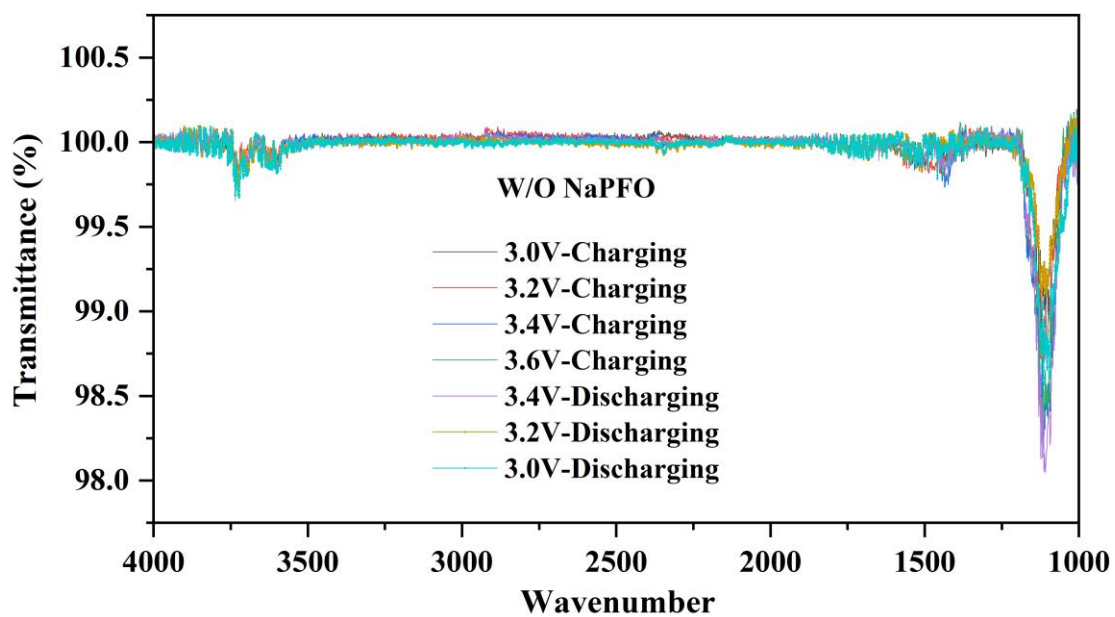
**Fig. S18.** Long-term cycling performance of Li||LFP cells using LiFSI/THF, LiFSI-NaPFO/THF and LiPF<sub>6</sub>/EC+DEC at 15.0 C rate.



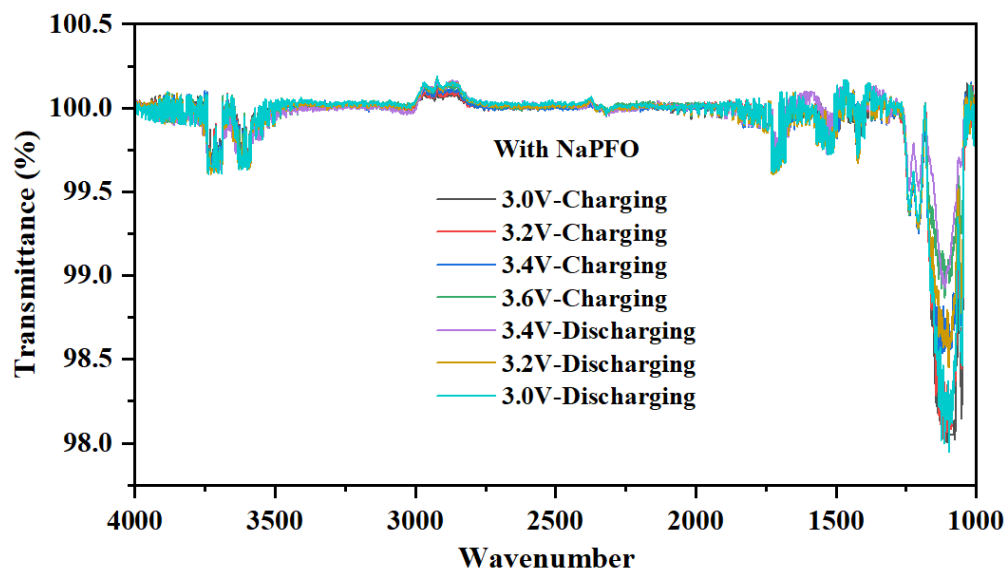
**Fig. S19.** (a) Three-Electrode long cycling study of LFP||Li||Li cells at 15.0 C. Voltage curves of the LFP cathodes with respect to the lithium foil reference electrodes after (a) 50 cycles and (b) 2000cycles.



**Fig. S20.** In situ ATR-SEIRAS spectra under 3.0 V (vs. Li/ Li<sup>+</sup>) for the two electrolytes system in the range of 4000-1000 cm<sup>-1</sup>.



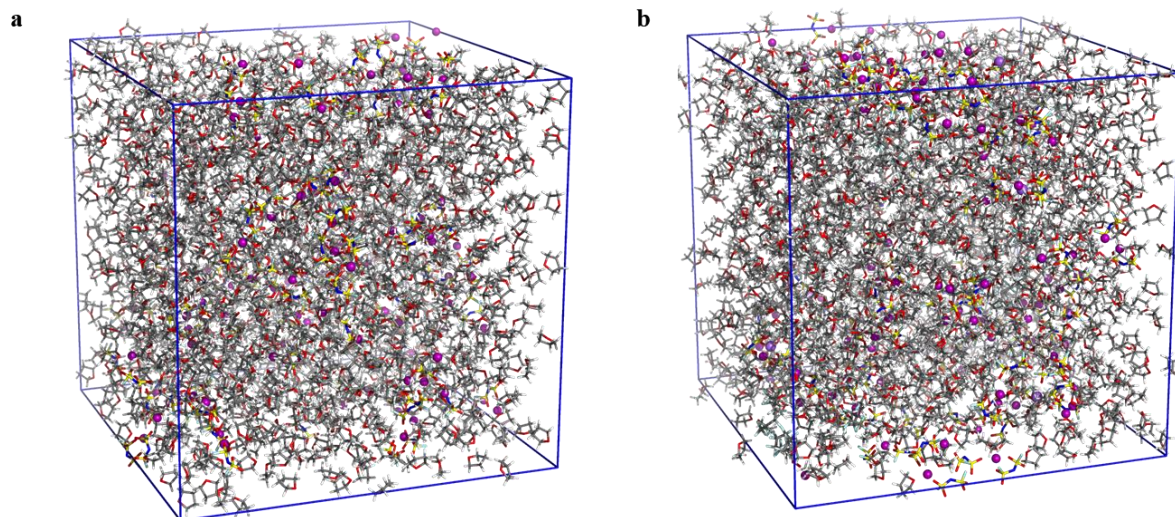
**Fig. S21.** In situ ATR-SEIRAS spectra under various potentials for the LiFSI/THF electrolytes in the range of 4000-1000 cm<sup>-1</sup>.



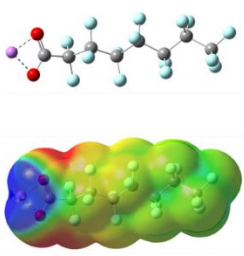
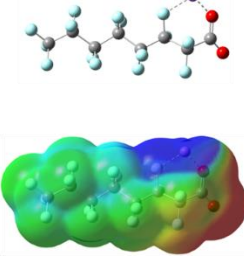
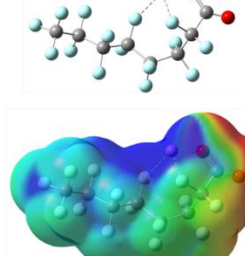
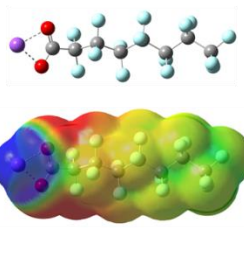
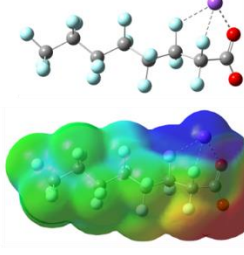
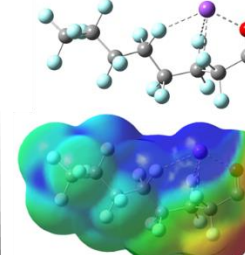
**Fig. S22.** In situ ATR-SEIRAS spectra under various potentials for the NaPFO-containing system in the range of 4000-1000  $\text{cm}^{-1}$ .



**Fig. S23.** Optical images of 2% wt NaPFO in THF and 1M LiFSI+2%wt NaPFO in THF.



**Fig. S24.** The MD snap shot of LiFSI/THF (a) and LiFSI-NaPFO/THF (b).

<b>Li-PFO</b>			
<b>Binding Energy (eV)</b>	<b>-6.64904</b>	<b>-6.40927</b>	<b>-6.55827</b>
<b>Na-PFO</b>			
<b>Binding Energy (eV)</b>	<b>-5.42018</b>	<b>-5.46645</b>	<b>-5.52492</b>

**Fig. S25.** Interaction form and corresponding binding energy between lithium ion/sodium ion and PFO<sup>-</sup> anions.

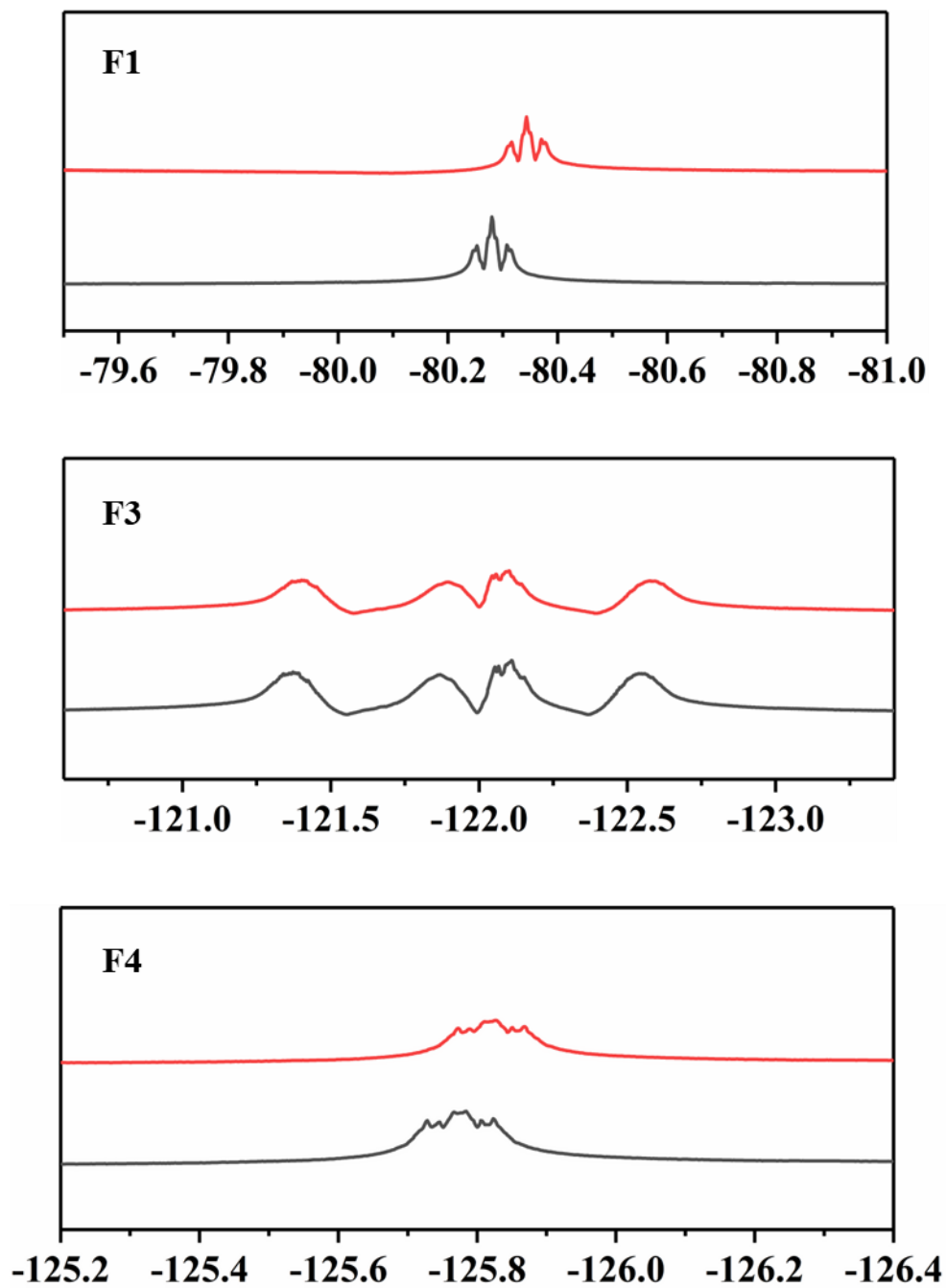


**Fig. S26.** The chemical shift of F1, F3, F4 at NaPFO in NaPFO/DMSO solution with and without LiFSI.

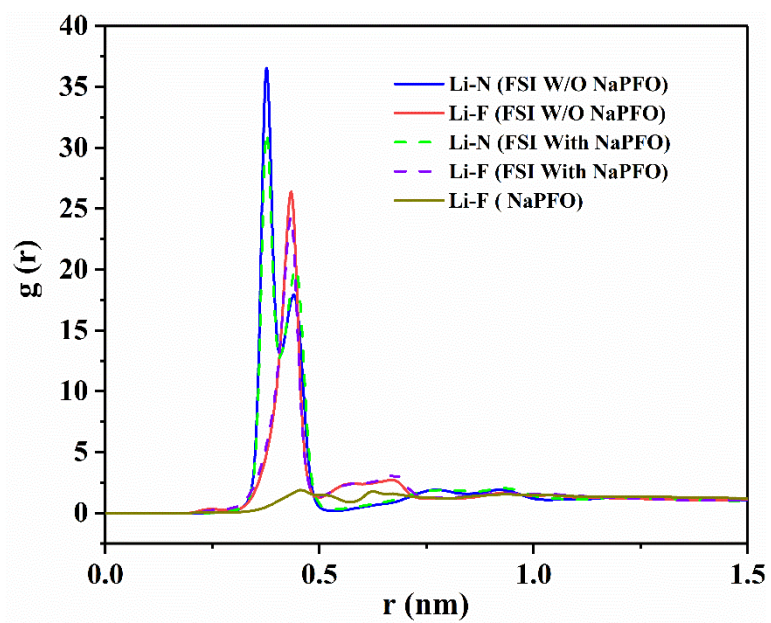


**Fig. S27.** The radial distribution of  $\text{Li}^+$  ions in blank and NaPFO-contained electrolyte systems.

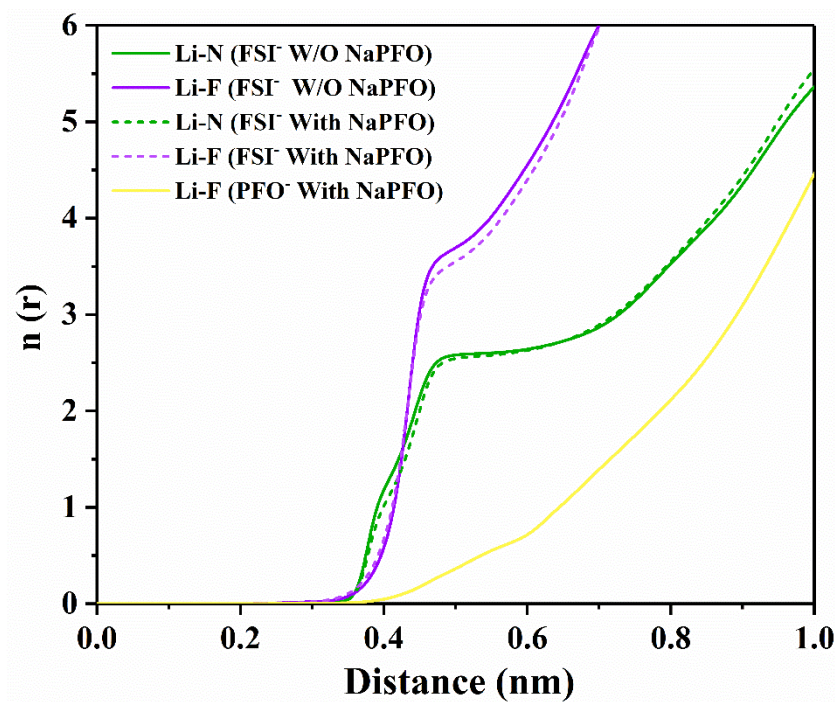


**Fig. S28.** The coordination number of  $\text{Li}^+$  ions in blank and NaPFO-contained electrolyte systems.

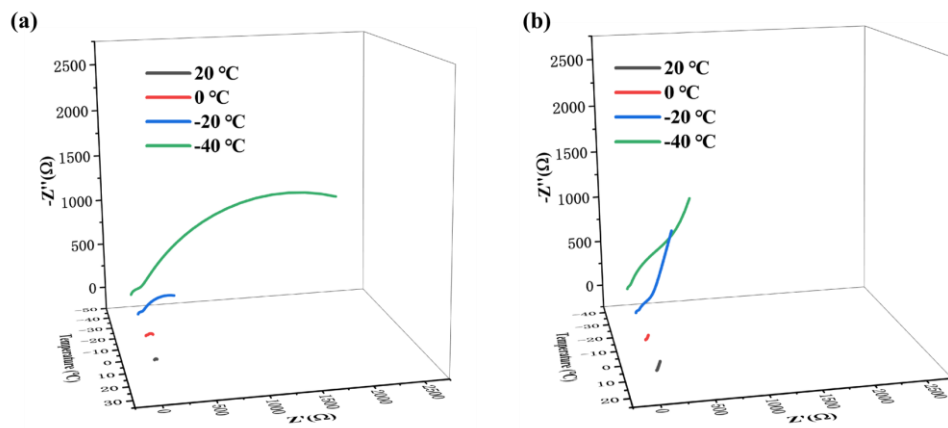


**Fig. S29.** Impedance spectra of the NMC811 cathode in LiFSI/THF (a) and LiFSI-NaPFO/THF (b) at 50% state-of-charge (SOC) at different temperature.

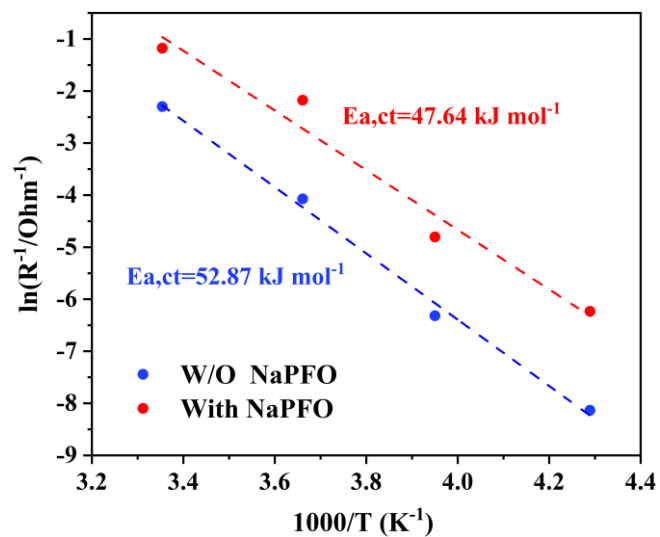


**Fig. S30.** Arrhe-nius behavior of the resistance corresponding to Li<sup>+</sup> desolvation at cathode using 3-electrode cell.

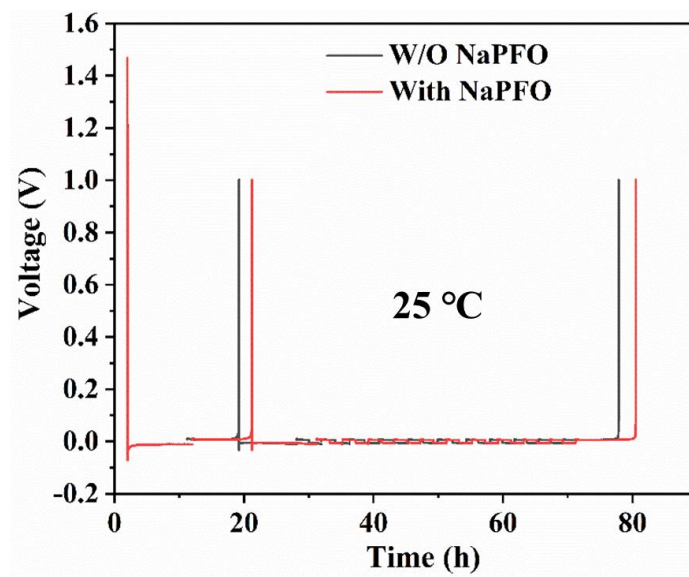


**Fig. S31.** Aurbach CE of Li||Cu cells at 25 °C.

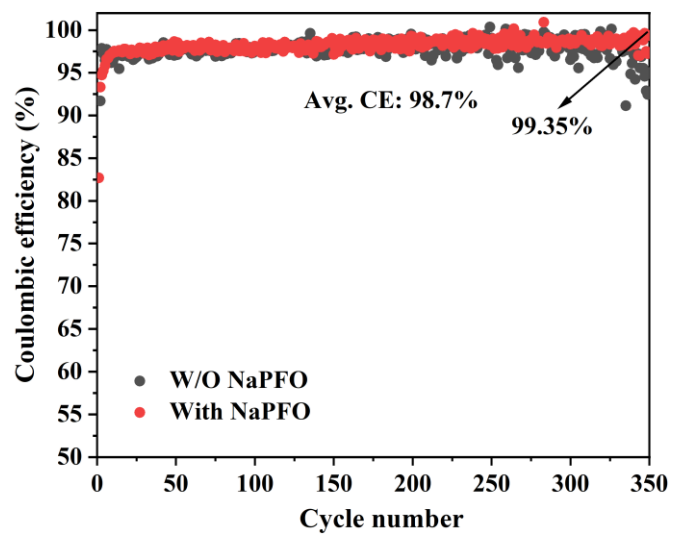


**Fig. S32.** Cycling CE of Li||Cu cells (1mA, 1mAh).

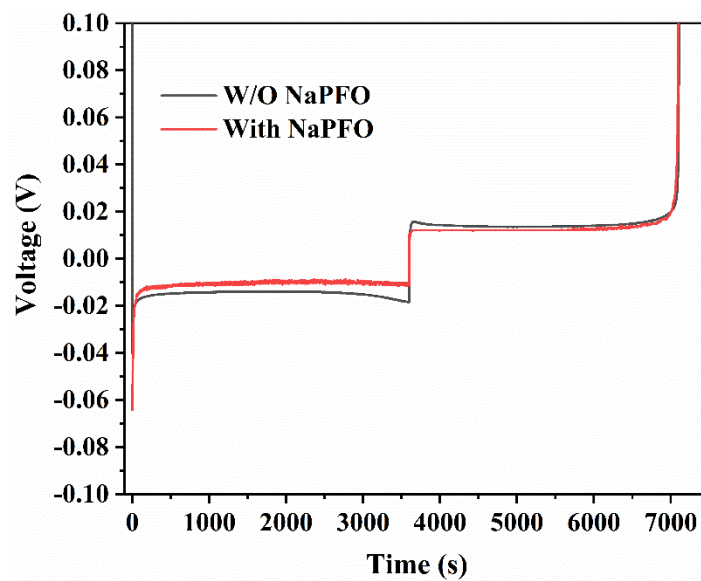


**Fig. S33.** Voltage profiles of Li||Cu cells cycled in LiFSI/THF and LiFSI-NaPFO/THF.

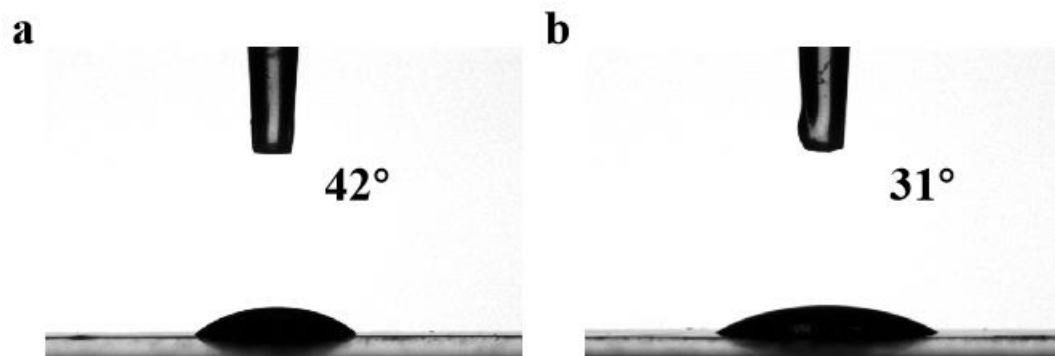


**Fig. S34.** Wettability of the separators in the LiFSI/THF (a) and LiFSI-NaPFO/THF (b).

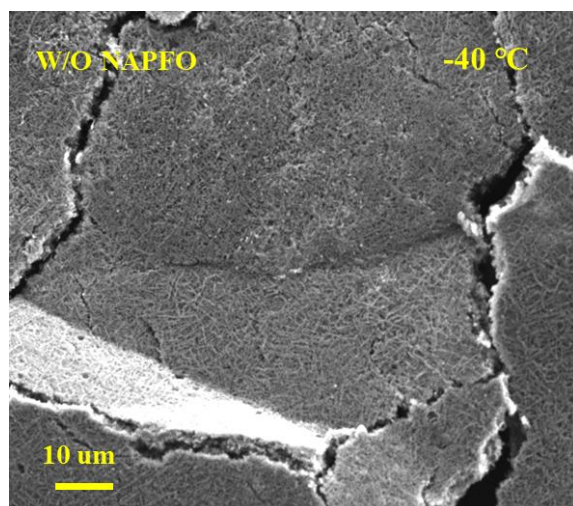


**Fig. S35.** SEM images of Li plated in LiFSI/THF at -40 °C.

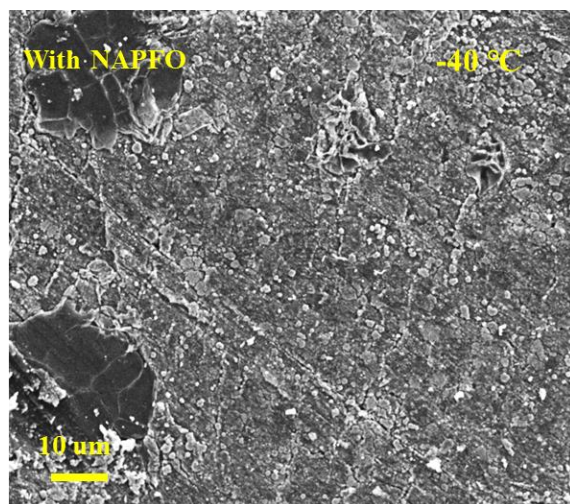


**Fig. S36.** SEM images of Li plated in LiFSI-NaPFO/THF at -40 °C.

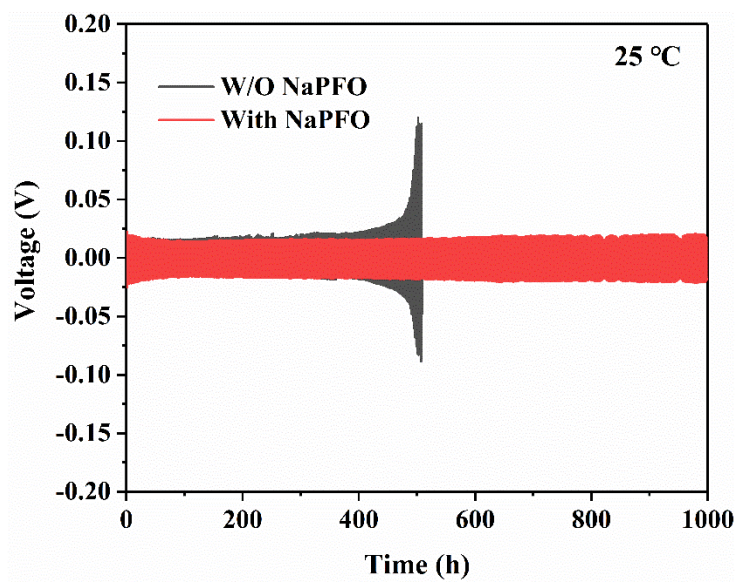


**Fig. S37.** Li||Li cell cycled in LiFSI/THF and LiFSI-NaPFO/THF at 25 °C.

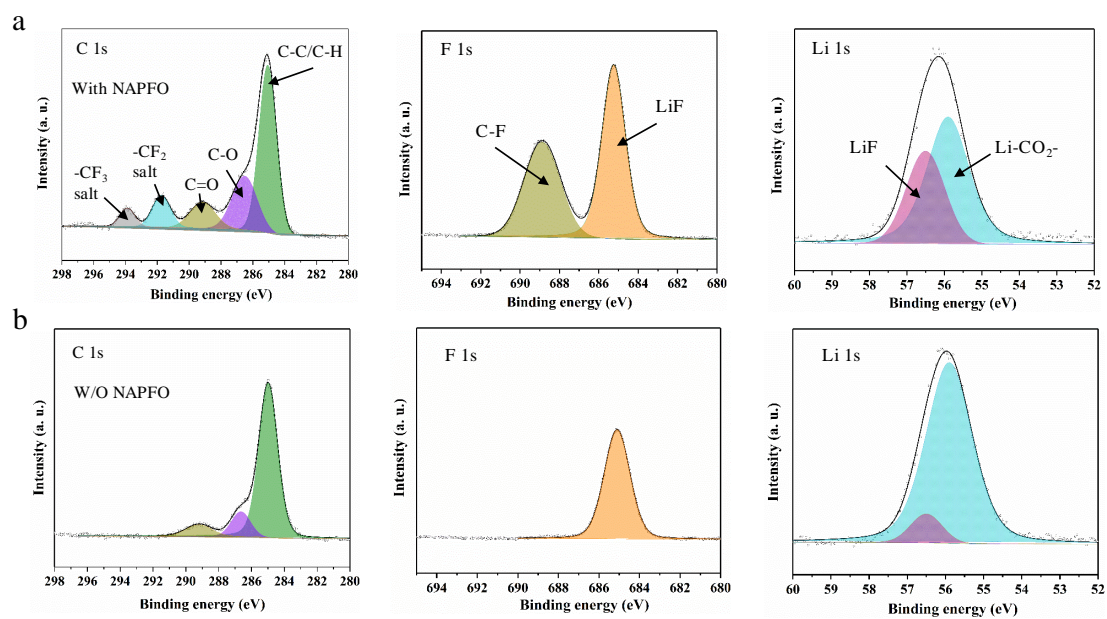


**Fig. S38.** X-ray photoelectron spectroscopy (XPS) profiles of C1s, F1s and Li1s of SEI formed on Lithium metal surface cycled in LiFSI-NaPFO/THF (a) and LiFSI/THF (b) after 20 cycles.

## Supplementary Note 1

It should be mentioned here that 2 wt % TMSP were introduced in LiFSI-NaPFO/THF for better battery performance. We found that the introduction of TMSP, a film forming additive commonly used for cathodes, further improved the capacity and long cycle stability of Li||NMC811 cells. As shown in Fig. S41-43, Li||NMC811 cells using LiFSI-NaPFO/THF+TMSP exhibited the highest specific capacity and more stable long cycle performance at the charge/discharge rate of 0.5 C, 1.0 C and 2.0 C. Li||NMC811 cells using LiFSI-NaPFO/THF+TMSP also exhibit the best rate characteristics (Fig. S44). The above results indicate that the combination of sacrificial additive TMSP and adsorption additive NaPFO will help the battery to achieve optimal performance. Therefore, the LiFSI/THF+TMSP electrolyte system will be used as the blank control for the testing of full cells and pouch cells in this article.

In addition, we conducted additional EQCM experiments on the 1M LiFSI+NaPFO/THF+TMSP electrolyte system. The results show that in the electrolyte system containing TMSP, a conventional additive for CEI formation, we observed similar phenomena to those in the 1M LiFSI+NaPFO/THF system without TMSP. During charging (voltage rising from 3.0 V to 3.6 V), the D value (a stiffness indicator) decreases as the voltage increases, indicating that the adsorption layer at the interface becomes stiffer due to the effect of the electric field (Fig. S45). This phenomenon suggests that the PFO<sup>-</sup> anions gradually transition from a disordered to an ordered assembly under the influence of the electric field. When the voltage is

discharged from 3.6 V back to 3.0 V, the D value increases again, indicating a softening of the adsorption layer and revealing the reversibility of the structural orientation changes of PFO<sup>-</sup> caused by the electric field. Therefore, EQCM results show that the introduction of TMSP did not affect the adsorption behavior of NaPFO at the interface.

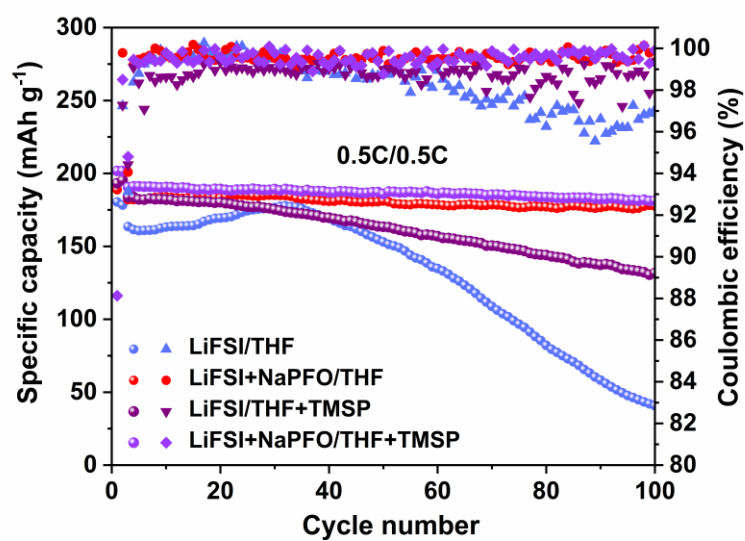


**Fig. S39.** Long-term cycling performance of Li||NMC811 cells using LiFSI/THF, LiFSI+NaPFO/THF, LiFSI/THF+TMSP and LiFSI+NaPFO/THF+TMSP at 0.5 C rate.

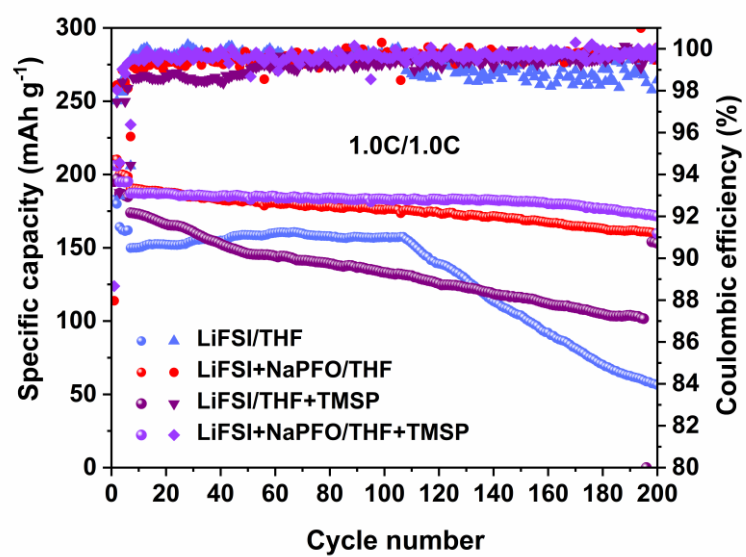


**Fig. S40.** Long-term cycling performance of Li||NMC811 cells using LiFSI/THF, LiFSI-NaPFO/THF, LiFSI/THF+TMSP and LiFSI-NaPFO/THF+TMSP at 1.0 C rate.

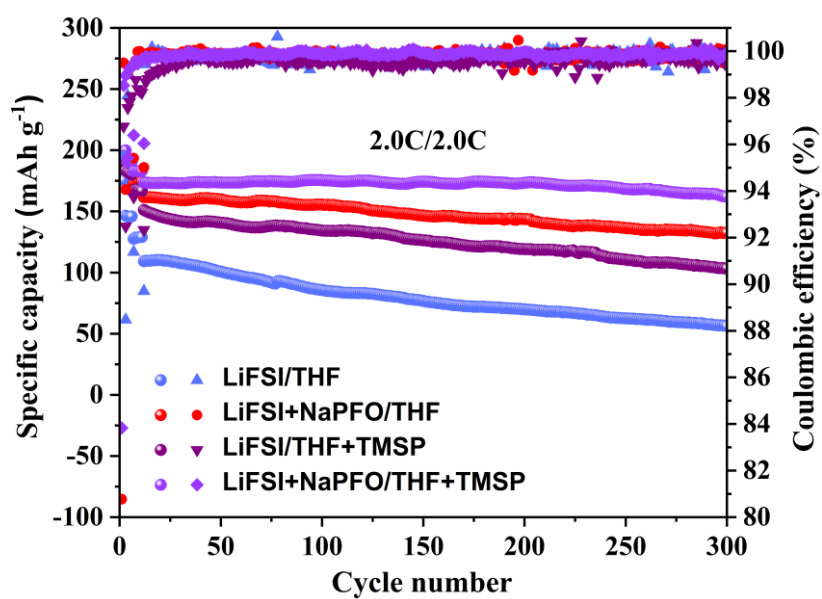


**Fig. S41.** Long-term cycling performance of Li||NMC811 cells using LiFSI/THF, LiFSI-NaPFO/THF, LiFSI/THF+TMSP and LiFSI-NaPFO/THF+TMSP at 2.0 C rate.

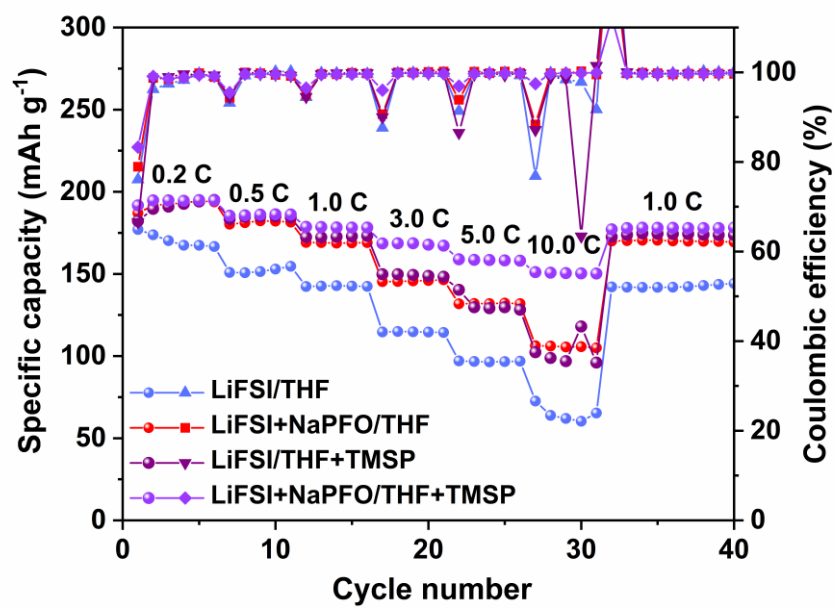


**Fig. S42.** Rate performance of Li||NMC811 cells using LiFSI/THF, LiFSI-NaPFO/THF, LiFSI/THF+TMSP and LiFSI-NaPFO/THF+TMSP.

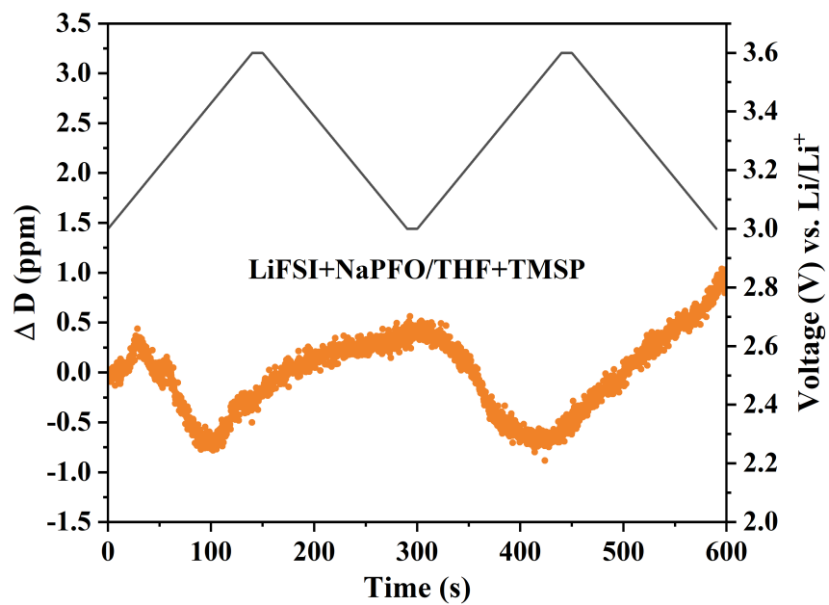


**Fig. S43.** The dissipative factor-Time curves of working electrode interface during the GCD process with LiFSI+NaPFO/THF+TMSP electrolyte characterized by EQCM.

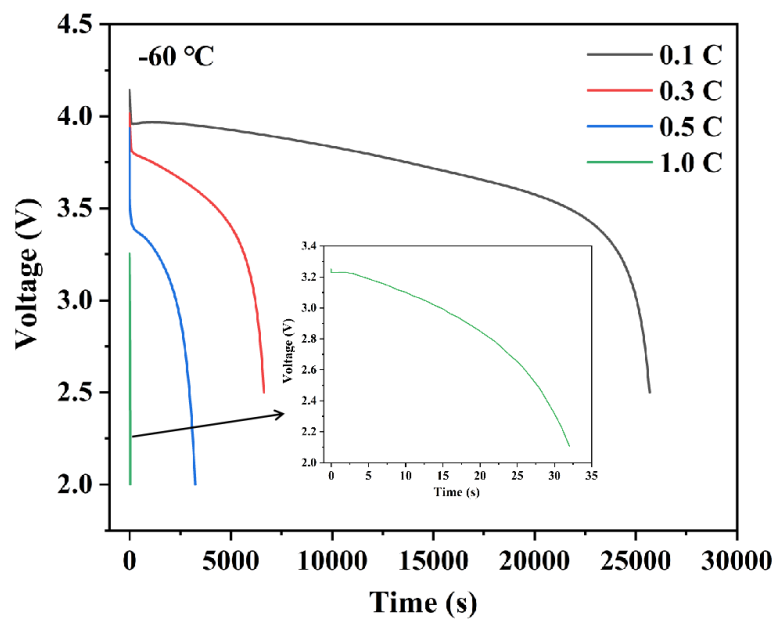


**Fig. S44.** Discharge curves at different rate of 500 mAh pouch cells under -60 °C.

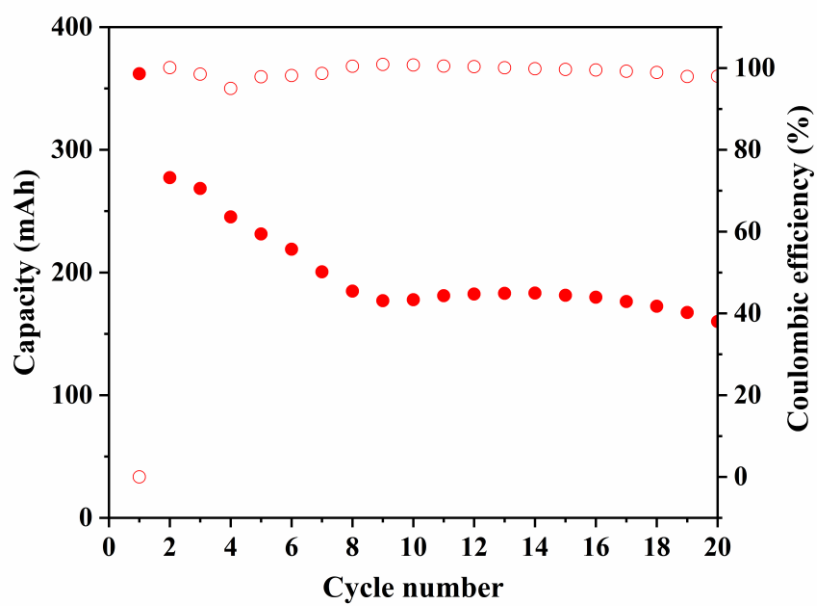


**Fig. S45.** Long-term cycling performance of 500 mAh Li||NMC811 pouch cells LiFSI-NaPFO/THF+TMSP at -40 °C.

## Supplementary Note 2

Before conducting in situ EQCM testing, we measured the LSV curve of the electrolyte using a nickel-plated gold chip as the working electrode and lithium metal as the counter and reference electrode. We observed that the potential for irreversible decomposition of both bare electrolyte and LiFSI-NaPFO/THF (including CEI formation) exceeds 4.0 V. No irreversible redox peaks were observed in the potential range of 3.0-3.6V (vs. Li/Li<sup>+</sup>), as shown in Fig. S48 inset. In addition, the perfect symmetrical triangular shape of the charging and discharging curve demonstrates the pure capacitive behavior during the entire charging and discharging process (new Fig. S 3f). Therefore, for EC-QCM testing, we strictly control the potential between 3.0 and 3.6 V (vs. Li/Li<sup>+</sup>) throughout the whole measurement process to ensure that the electrode interface only undergoes pure capacitive behavior of ion adsorption and desorption without any Faraday reaction (CEI formation) involved.

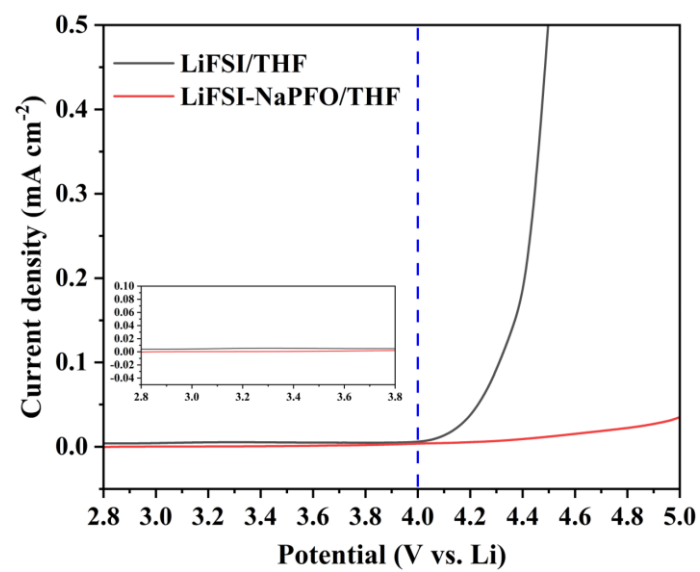


**Fig. S46.** LSV curves of Li/nickel plated gold chip cells in both electrolytes.

### Supplementary Note 3

Before conducting in situ AFM testing, we first measured the LSV curve of the electrolyte (LiFSI-NaPFO/THF) using a gold chip as the working electrode and lithium as the reference electrode. We observed that the current density slowly increases when the potential exceeds 4.2 V (vs. Li/Li<sup>+</sup>), which may be due to the irreversible decomposition of electrolytes to form CEI as reported before. Therefore, the potential of the working electrode during the EC-AFM testing was strictly cycled between 3.0 V and 3.6 V throughout the whole measurement process to ensure that the electrode interface only undergoes pure capacitive behavior of ion adsorption and desorption without any Faraday reaction involved in the CEI formation.

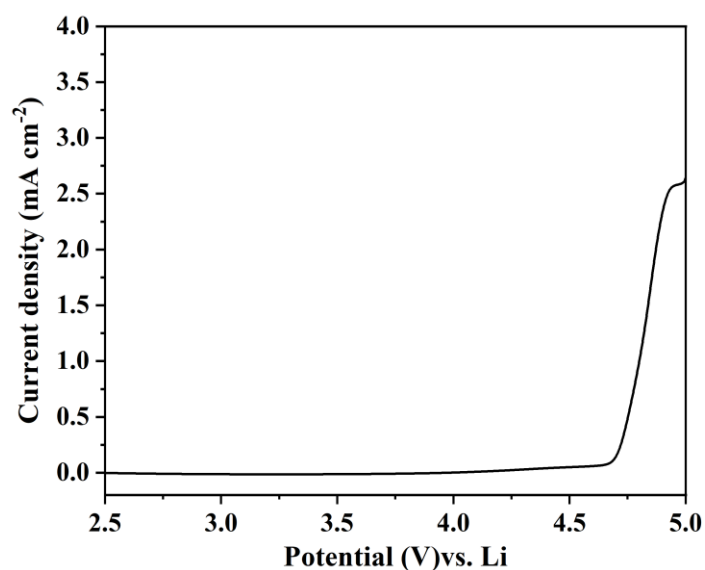


**Fig. S47.** LSV curves of Li/gold chip cells in LiFSI-NaPFO/THF electrolytes.

Supplementary Table 1. Comparison of our work with recent electrolyte works on the energy density and power density lithium metal batteries at ultra-low temperature.

<b>Electrolyte</b>	<b>Cell condition</b>	<b>Cutoff voltage (vs Li/Li<sup>+</sup>)</b>	<b>(Maximum) Energy density at low temperature</b>	<b>(Maximum) Power Density at low temperature</b>
1M LiFSI DEE	Li  SPAN pouch cell	3.5V	143 Wh kg <sup>-1</sup> at -40 °C 126 Wh kg <sup>-1</sup> at -60 °C	17.2 W kg <sup>-1</sup> at -40 °C (calculated) 16.5 W kg <sup>-1</sup> at -60 °C (calculated)
1 M LiFSI BTFE/DME (5 : 1 vol%)	Li  NMC811 pouch cell	4.3V	230 Wh kg <sup>-1</sup> at -40 °C	23 W kg <sup>-1</sup> at -40 °C (calculated)
1.0 M LiFSI DiFEC/ MTFC/HFME (1:2:2 vol%)	Graphite  NMC523 pouch cell	4.6V	270 Wh kg <sup>-1</sup> at -40 °C	16.5 W kg <sup>-1</sup> at -40 °C (calculated)
1.0 M LiFSI THF+0.5% wt NaPFO+2% wt TMSP	Li  NMC811 pouch cell	4.3V	327 Wh kg <sup>-1</sup> at -40 °C 301 Wh kg <sup>-1</sup> at -60 °C	359 W kg <sup>-1</sup> at -40 °C 318 W kg <sup>-1</sup> at -60 °C

## References

1. Y. Wang, F. U. Shah, S. Glavatskih, O. N. Antzutkin, A. Laaksonen, J. Phys. Chem. B 2014, 118, 8711.
2. M. J. Abraham, T. Murtola, R. Schulz, S. Páll, J. C. Smith, B. Hess, E. Lindahl, SoftwareX 2015, 1, 19.